# High-resolution depth imaging of long-offset 2D data using full-waveform inversion: The Malvinas Basin, Argentina

Laurence Letki[1], Mike Saunders[2], Monica Hoppe[3], Milos Cvetkovic[2], Lewis Goss[3], and Ahmed Rady[2]

https://doi.org/10.1190/tle38030220.1.






## Abstract

The Argentina Austral Malvinas survey comprises 13,784 km of 2D data extending from the shelf to the border with the Falkland Islands. The survey was acquired using a 12,000 m streamer and continuous recording technology and was processed through a comprehensive broadband prestack depth migration workflow focused on producing a high-resolution, high-fidelity data set. Source- and receiver-side deghosting to maximize the bandwidth of the data was an essential ingredient in the preprocessing. Following the broadband processing sequence, a depth-imaging workflow was implemented, with the initial model built using a time tomography approach. Several passes of anisotropic reflection tomography provided a significant improvement in the velocity model prior to full-waveform inversion (FWI). Using long offsets, FWI made use of additional information contained in the recorded wavefield, including the refracted and diving wave energy. FWI resolved more detailed velocity variations both in the shallow and deeper section and culminated in an improved seismic image.


## Introduction

The Malvinas Basin lies offshore Argentina, east of Tierra del Fuego, between the Dungeness Arch and the Malvinas (Falkland) Islands and is attached to the North Scotia transform boundary (Galeazzi, 1998) (Figure 1). The Malvinas Basin is mapped as a triangular depocenter extending for some 300 km north–south and 350 km east–west at its southern boundary along the fold belt paralleling the North Scotia transform fault. The wedge-shaped basin reaches a maximum depth of approximately 10,000 m at its deepest point, with a sedimentary fill of Jurassic- to Holocene-aged succession of mostly mud-prone marine siliciclastic strata.

The evolution of the Malvinas Basin consisted of three main phases typical of a passive tectonic margin: rift, sag, and foredeep (Galeazzi, 1998). Grabens oriented in a north–northwest direction were created during Jurassic-aged rifting and were filled with continental sediments of volcanic and pyroclastic origin. During the Late Jurassic sag phase, there was diminished faulting with generalized subsidence accompanied by the deposition of a basal transgressive marine wedge. The tectonically quiescent Late Cretaceous interval generated mud-prone offshore sedimentation, and by the early Paleogene the development of the foredeep trough was initiated by transtentional tectonism. The basin was partially filled with outer shelf glauconite-rich sandstones, basinal claystones, and localized carbonate buildups. The actual foredeep phase was initiated by a strong deepening event in the middle Eocene-Oligocene, resulting in the development of the Malvinas foredeep. This phase also resulted in the formation of compressional structures in the foreland.

The Argentina Austral Malvinas survey comprises 13,784 km of 2D data extending from the shelf to the border with the Falkland Islands (Figure 2). The survey was acquired using a 12,000 m streamer and continuous recording technology, resulting in a data set with excellent imaging from the mudline to the deep basement. The acquisition parameters are summarized in Table 1.

The data were processed through a comprehensive broadband prestack depth migration workflow. In this paper, we review the key steps of this processing sequence with an emphasis on full-waveform inversion (FWI) as a standard part of the model-building workflow.

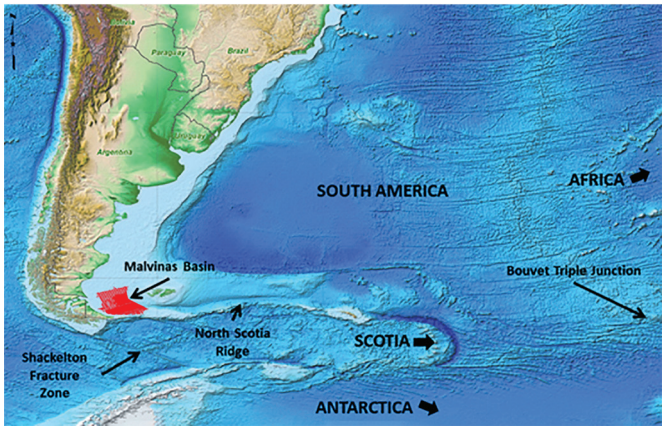


**Figure 1.** Tectonic map of the Malvinas Basin.

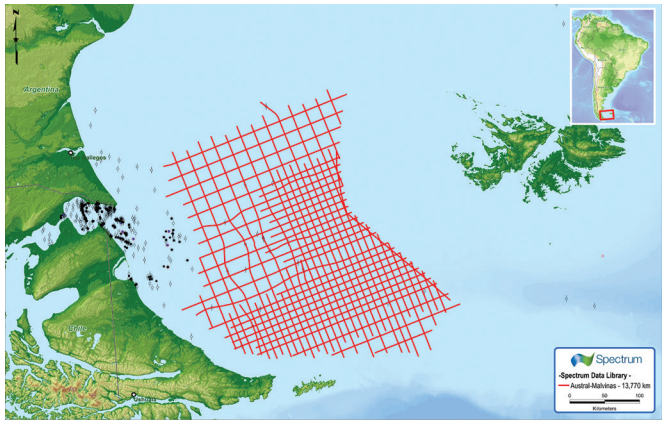


**Figure 2.** Map showing survey coverage.

[1]DownUnder GeoSolutions Pty. Ltd., London, UK. E-mail: laurencel@dug.com.
[2]Spectrum Geo Inc., Multi-Client, Houston, Texas, USA. E-mail: mike.saunders@spectrumgeo.com; milos.cvetkovic@spectrumgeo.com; ahmed.ra.rady@gmail.com.
[3]DownUnder Geosolutions Pty. Ltd., Houston, Texas, USA. E-mail: monicah@dug.com; taylorg@dug.com.

As the seismic industry redefines itself, modern 2D exploration programs require more economically efficient business models. The integration of geologic and geophysical workflows has proven to be a successful strategy to achieve this for large-scale multiclient programs in frontier basins (Cvetkovic et al., 2016). The time and depth velocity model-building workflow applied to this program presents a robust methodology that provides reliable models while reducing the overall timeline.

## Processing sequence overview

The processing sequence consisted of several major stages:

- Initial data quality control
- Noise attenuation
- Source- and receiver-side deghosting
- Free-surface multiple attenuation
- Velocity model building, including reflection tomography and FWI
- Anisotropic prestack depth migration
- Postmigration data conditioning, including residual multiple attenuation, residual moveout correction (RMO), and absorption correction

## Broadband preprocessing

Streamer seismic data have inherent bandwidth limitations caused by the interference of free-surface ghosts with the primary reflections of interest. To ensure a high-resolution, high-fidelity image of the ghost-free primary wavefield for structural, stratigraphic, and quantitative interpretation, it is crucial to preserve and maximize bandwidth with a broadband processing strategy. A deterministic deghosting algorithm was used to correct the amplitude and phase distortion caused by both the source and receiver ghosts, resulting in a broader spectrum at the high and low ends (Figure 3). Of course, bandwidth has direct implications on the bed thickness that can be resolved in the final image.

The deghosting process formulates the forward ghost model using the wave equation in the $f$-$p$ domain, accounting for arbitrary receiver and source depth profiles and a directional expression of stochastic free-surface reflectivity. The Radon transform handles variable trace spacing, and a radial symmetry is imposed by using the Euclidean distances between source and receiver. To the extent that radial symmetry is fulfilled, the algorithm is perfectly correct in 3D. The forward model is expressed as the system of equations $\mathbf{Gu} = \mathbf{d}$ in which the observed data, $\mathbf{d}$, and the forward ghost modeling operator, $\mathbf{G}$, are used to invert for the upcoming wavefield, $\mathbf{u}$, at the free surface for each frequency. The system is solved in a least-squares sense using robust conjugate gradient methods so that all events, offsets, and dips are accurately deghosted.

Following deghosting, attention was given to the demultiple workflow while maintaining focus on the broadband strategy. After building a model of 2D surface-related multiples, the model was adaptively subtracted from the input data over two discrete frequency bands with parameters adjusted to optimize the results at the low and high ends of the spectrum, respectively.

## Velocity model building

The velocity model-building strategy consisted of three main steps. Initially, a time-domain velocity model is built and refined before being converted to depth. Using this initial model, reflection tomography, constrained with calibrated borehole data, was used in an iterative workflow to generate a vertically transverse isotropy (VTI) anisotropic model. Finally, this model was further refined via an FWI workflow that resulted in an improved seismic image. It is important to note that this workflow was implemented on a largely unexplored basin covering 500,000 km$^2$ on a production timeline.

***Initial model.*** An initial time-domain velocity model was built on a coarse grid, with manual velocities on vertical semblance at 5 km spacing, which was then used as input to time tomography.

Anisotropic time tomography updates a VTI migration velocity field using a set of RMO picks, using all available offsets, with the objective of providing a geologically consistent

**Table 1.** Argentina Austral Malvinas survey.

| Acquisition parameters | |
|---|---|
| Start date | 13 November 2017 |
| End date | 8 March 2018 |
| Total survey length | 13,784 km |
| Source volume/pressure | 4230 in$^3$/2000 psi |
| Source array configuration | 3 × 12 gun subarrays/15 m length/8 m separation |
| Source depth | 8 m |
| SP interval | 25 m |
| Record length | 15 s |
| Streamer length | 12,000 m |
| Streamer depth | 13 m |
| Sample interval | 2 ms |
| Recording low-cut filter | 3 Hz at 6 dB/octave |
| Recording high-cut filter | 200 Hz at 370 dB/octave |

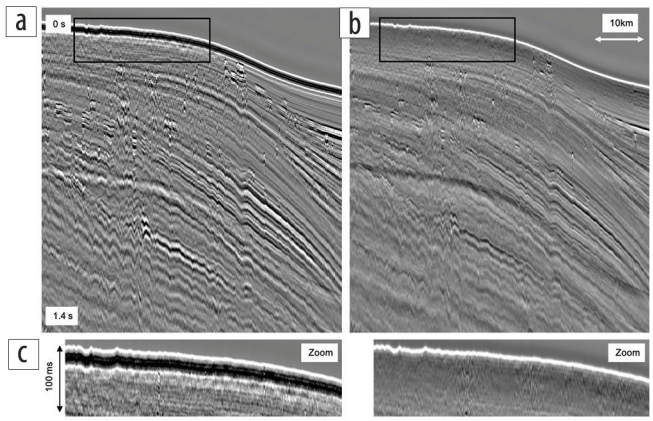


**Figure 3.** Example stacks (a) before and (b) after source and receiver deghosting highlighting the increase in resolution as the ghost interferences are removed. Note that no demultiple has been applied yet to the data at this stage of the processing. (c) Corresponding zoom sections around the highlighted part of the water bottom.

update to an initial migration velocity field. If no eta model (one of the Thomsen anisotropic parameters) exists, an initial eta volume will be produced, or the eta volume will be updated during subsequent passes of tomography. The time tomography workflow is very similar to a depth tomography workflow, in the sense that an objective function is inverted at each trace location using three major constraints (based on the ideas presented in Koren and Raave, 2006). This process is applied simultaneously to both velocity and eta fields. The first constraint honors the RMO picks ensuring that the two-way-time/offset relationship implied by the inverted models is consistent with the observed relationship defined by the picks. The second constraint minimizes deviations from a smooth background interval model (for both velocity and eta, respectively) implied by the inputs (initial models and RMO picks). The third constraint inhibits oscillations forming in the output interval models. The nonorthogonality of eta and velocity means they should be updated simultaneously to minimize leakage between the two. The constraints in the tomography ensure a geologically consistent eta and interval velocity, simultaneously.

In total, three iterations of time tomography were applied at 100 m horizontal grid intervals. This velocity model was then converted to the depth domain and, after inserting a water velocity profile based on the "Hood" function (Advocate and Hood, 1993), became the initial depth velocity model.

***High-resolution tomography.*** Traveltime ray-based reflection tomography is an optimization algorithm that updates velocity model parameters with the objective of minimizing the RMO observed on image gathers. In this survey, a combination of volume-based and horizon-based picks were used for the tomographic updates.

Tomography is both an overdetermined and underdetermined problem. That is, it is virtually impossible to make all the gathers flat with residuals equal to zero, yet there also exists an infinite space of models that would flatten the gathers to the same extent. Consequently, a regularization method is required to ensure the updates are geologically consistent. A regularization scheme that is geologic-structure aware is used to prevent excessive smoothing across interfaces, including those with dip. It restricts the space of available models by adopting an algorithm from the image reconstruction and FWI communities — total variation regularization. Structurally oriented regularization is applied in the construction of the total variation constraint itself, relying on the construction of a diffusion tensor field (Weickert, 1998). This type of regularization promotes structural continuity in the absence of other information while permitting abrupt changes where required. It encourages the tomography to generate contiguous regions of uniform model parameter updates, following the structure in the image, and with well-defined boundaries between them. This is what makes the tomography a high-resolution tomography, not just the density of the picks.

After initial passes of isotropic velocity updates, the anisotropy fields required to build the VTI model are created by integrating borehole information in the workflow. The Malvinas Basin includes 12 wells, drilled from 1981 to 2011, covering much of the survey area. These wells included high-quality checkshot surveys and digital sonic logs that were used to determine the anisotropy parameters. Preserving normal moveout velocity, a delta field was derived from the well information to ensure the checkshot velocities are consistent with the velocity model and that a good match in depth of the acoustic markers was obtained. The information was propagated along the lines using interpreted seismic horizons. An initial epsilon field was then estimated from the delta and eta

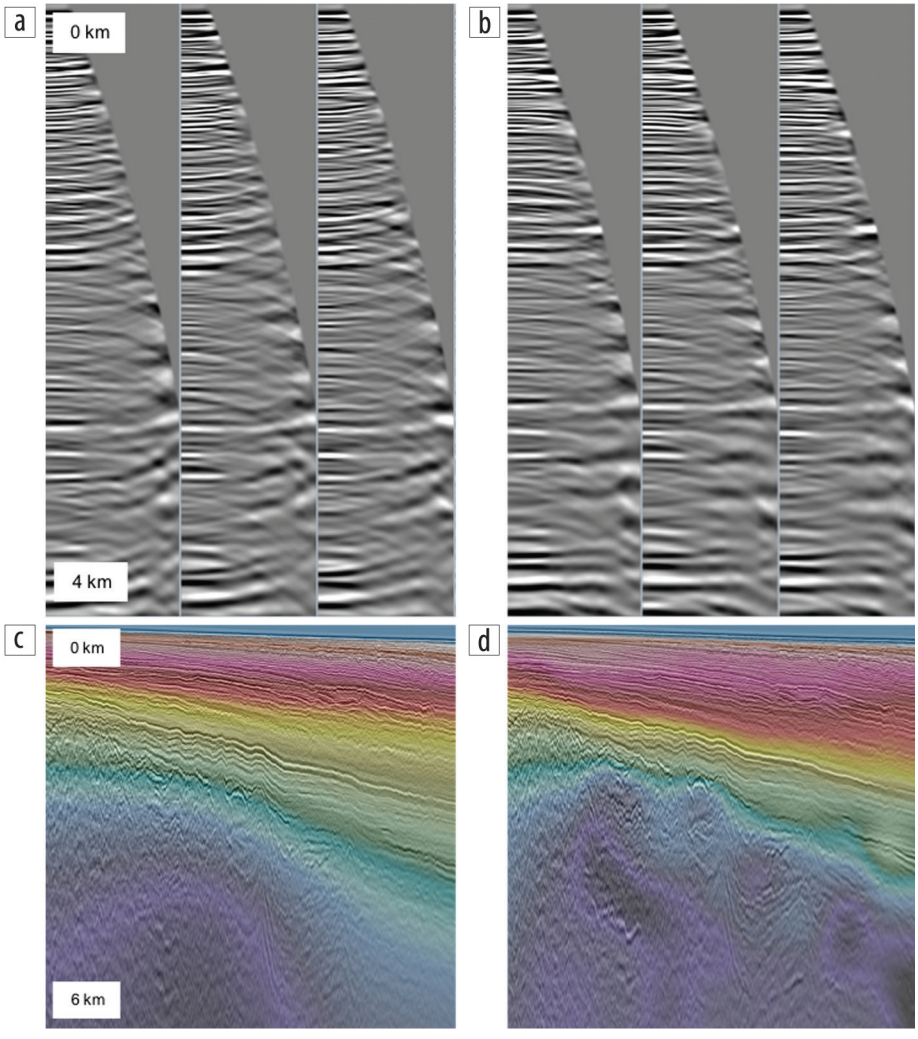


**Figure 4.** Representative image gathers using (a) the initial model and (b) the model after tomographic update showing a significant improvement in gather flatness. (c) and (d) The corresponding models with the migrated stack overlaid. The deeper structure initially not visible on the migrated stack is imaged with the updated model.

fields. The model was further updated using several iterations of anisotropic reflection tomography (see Figure 4).

***Full-waveform inversion.*** Although it is possible to obtain a detailed velocity model using ray-based reflection tomography, this technique makes use of only a small portion of the recorded wavefield — namely, the kinematics of the primary reflection data. By introducing FWI in the velocity model-building strategy, we can make use of information contained in the previously discarded refracted and diving waves. The algorithm is based on that described in Warner et al. (2013).

Figure 5 illustrates the FWI workflow. From a given velocity model, synthetic shot gathers are generated for the acquisition geometry using a forward modeling engine based on a two-way wave equation. It then back propagates the residual between the recorded seismic shot gathers and synthetic gathers to solve for model updates. The process is iterative, starting with the low-frequency content of the wavefield only and gradually moving toward including higher frequencies. It is important to note that the inversion will attempt to fit both the phase and amplitude spectra of the data. Amplitude effects that vary slowly in time down the traces are compensated for by sliding-window normalization. This compensates both for mild attenuation effects and the cylindrical geometric spreading implicit in the 2D modeling. Regarding cable feathering — another challenge associated with running FWI on 2D data — we assume that offset dominates azimuth in terms of its effect on the data. Therefore, receiver locations for each shot are shifted onto the 2D line in such a way that the real-world and modeled offsets are equal.

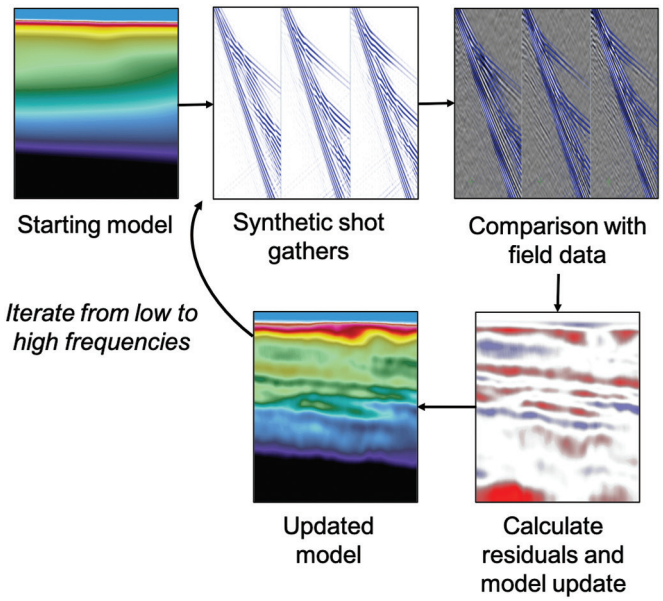


**Figure 5.** Overview of the FWI workflow.

As all free-surface effects, including ghost effects, will be modeled as part of the forward propagation, the shot gathers required for FWI were the raw field data, with minimum preprocessing applied to ensure that the lowest frequency in the data is carefully preserved. In terms of preconditioning, only a 1–2 Hz debias filter was applied to the data input to FWI.

One of the key requirements of the process is to obtain an accurate source wavelet. In this project, the modeled source wavelet proved unreliable, especially in the very low frequency range, so the source wavelet used for FWI was obtained from the direct arrival data.

To ensure that the process converges toward a global minimum, one must ensure that the initial synthetic data, modeled using the FWI starting model, matches the recorded data within half a cycle at the considered frequency. To ensure that this criterion is met and avoid cycle skipping, one must start the process at the lowest usable frequency and ensure that the starting model is close enough to the true model, including an accurate estimation of the anisotropic effects. In this case, when comparing the synthetic data with the recorded field data at the starting frequency range — up to 4 Hz — a strong mismatch was observed in the refracted part of the wavefield. The field data indicated the presence of a deep fast refractor not currently included in the model. The model was therefore manually updated prior to FWI to ensure a good initial match between synthetic and field data. Figure 6 demonstrates how including additional information can be extracted from previously ignored parts of the wavefield and highlights the potential of combining FWI with reflection tomography to optimize the model-building approach.

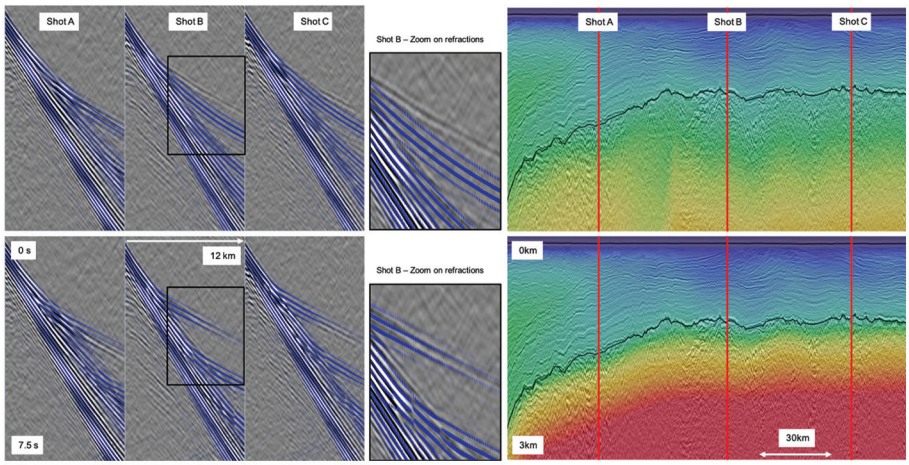


**Figure 6.** Synthetic shot gathers in dark blue overlaying recorded shot gathers in grayscale (left). When using the starting model (top right), a strong mismatch is observed in the refracted energy between synthetic and field data (top left). The FWI starting model has therefore been modified to include a stronger gradient below the horizon annotated in black (bottom right), leading to an improved match between synthetic and field data (bottom left).

The FWI approach applied on this data set is summarized as follows:

- First stage: gradually increasing the frequency content from up to 4 Hz, then 5 Hz, and finally 6 Hz, matching the data up to 6 km offset
- Long-wavelength anisotropic tomography update

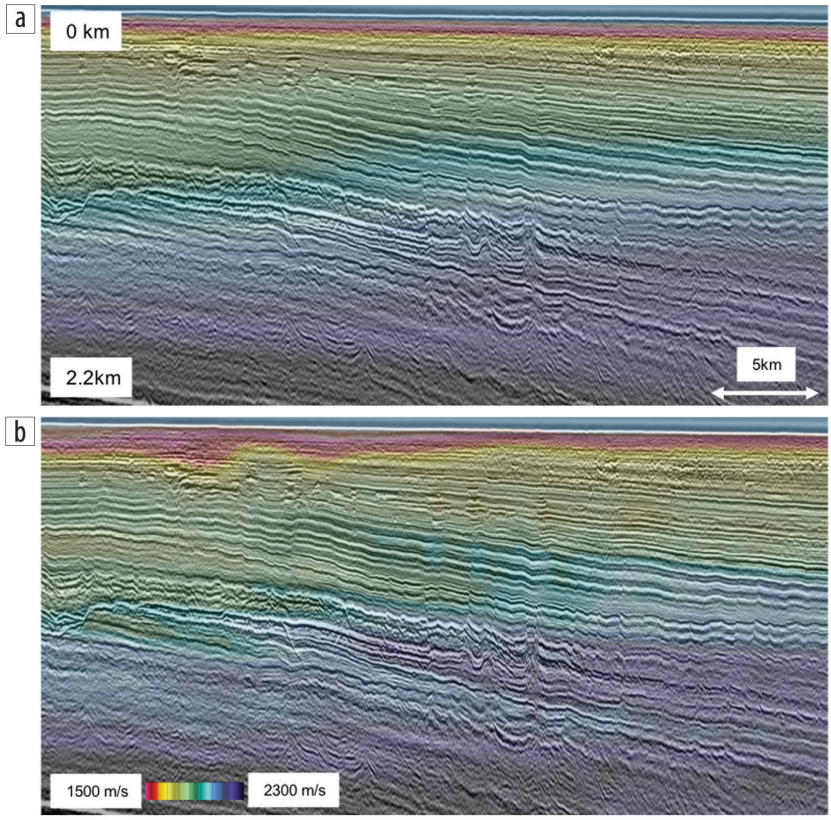


**Figure 7.** Velocity model (a) before and (b) after FWI update overlaid on corresponding migrated stack. In the FWI model, velocity details have been successfully resolved in the shallow section. The velocity anomalies and pinch outs are conformable with the underlying seismic data.

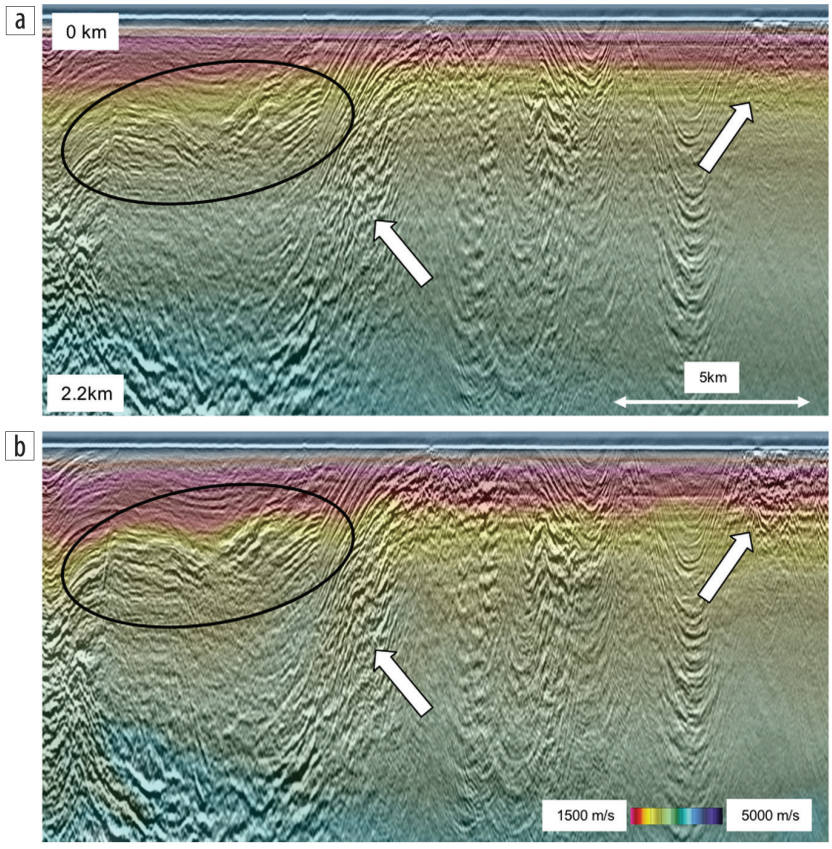


**Figure 8.** Velocity model (a) before and (b) after FWI update overlaid on corresponding migrated stack. In the FWI model, velocity details have been successfully resolved in the fold belt area in places where the tomography was not successful. The velocity is following the structure, and the seismic image is improved.

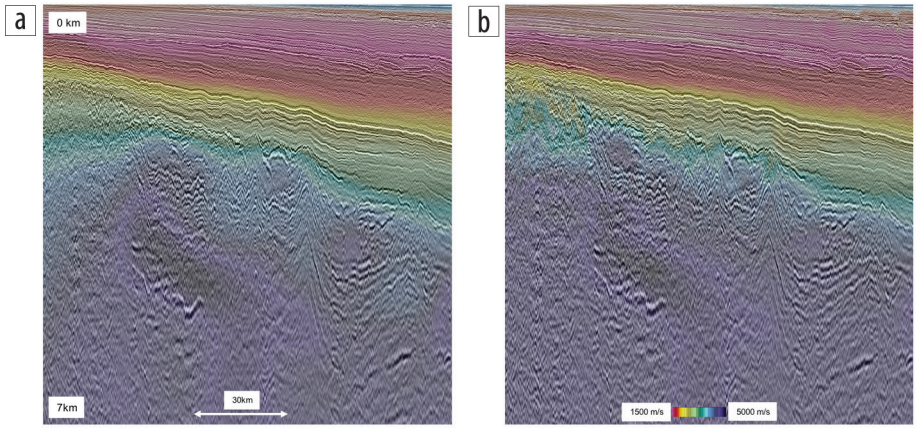


**Figure 9.** Velocity model (a) before and (b) after FWI update overlaid on corresponding migrated stack. With offsets of 12,000 m, FWI can resolve velocity details to a depth of 3–4 km.

- Second stage: using frequencies up to 6 Hz, matching the data up to 6 km offset, then gradually matching longer offsets (8 km, 10 km, and finally the full 12 km offset range) before increasing the frequencies to 7 Hz, 9 Hz, and finally 12 Hz
- A final long-wavelength anisotropic tomography update leads to the final velocity model used for anisotropic depth migration

Gradually increasing the offset included in the FWI was used as a pragmatic approach to improve the model in a traditional top/bottom approach and therefore avoid cycle skipping initially observed on the far-offset part of the data.

The maximum frequency used in the FWI was limited to 12 Hz. FWI can theoretically resolve details in the model up to half the seismic wavelength. For a fixed acoustic frequency, the wider the opening angle the lower the wavenumber of the velocity update. This means higher frequency transmitted/diving waves (which have very wide opening angles) can be used to get both long- and short-wavelength updates. That said, for imaging purposes, there typically are diminishing returns with increasing frequency because it is the lower frequencies that are the dominant control on the kinematics of the wavefield. The final frequency of 12 Hz was therefore appropriate for imaging using a Kirchhoff prestack depth migration.

Figures 7–9 show a comparison of the velocity model before and after FWI overlaid on the corresponding migrated stack image. In the FWI model, details of the velocity variations have been captured in the shallow sections, including localized areas of lower velocities and pinch outs, which show a very good conformity with the underlying seismic image. Details also have been captured much deeper in the section, from Lower Cretaceous, through the Springhill Formation, and up to the basement in certain parts of the survey area. Additional depths of updates are possible due to the availability of long-offset data, which ensures that the diving waves illuminating this deeper part of the subsurface have indeed been recorded and can therefore benefit the FWI updates.

## Summary

This case study demonstrates that a combination of broadband processing and state-of-the-art velocity model building, including FWI, can deliver the high-quality seismic image necessary for identification, mapping, and assessment of prospective targets. It also highlights the successful utilization of FWI in a production processing workflow for a large-scale, modern 2D exploration program.

Not only is there value in the final seismic image, but the higher resolution FWI-derived velocity model itself is also a very useful product with utility in a variety of quantitative interpretation workflows such as pore pressure prediction. TLE

## Data and materials availability

Data associated with this research are confidential and cannot be released.

Corresponding author: milos.cvetkovic@spectrumgeo.com

## References

Advocate, D. M., and K. C. Hood, 1993, An empirical time-depth model for calculating water depth, northwest Gulf of Mexico: Geo-Marine Letters, **13**, no. 4, 207–211, https://doi.org/10.1007/BF01207749.

Cvetkovic, M., L. Geiger, R. Clarke, C. Arias, O. Ramirez, S. Ward, and T. Seher, 2016, Integrated workflow for modern 2D programs in frontier areas: 86th Annual International Meeting, SEG, Expanded Abstracts, 280–284, https://doi.org/10.1190/segam2016-13972632.1.

Galeazzi, J. S., 1998, Structural and stratigraphic evolution of the Western Malvinas Basin, Argentina: AAPG Bulletin, **82**, no. 4, 596–636.

Koren, Z., and I. Ravve, 2006, Constrained Dix inversion: Geophysics, **71**, no. 6, R113–R130, https://doi.org/10.1190/1.2348763.

Warner, M., A. Ratcliffe, T. Nangoo, J. Morgan, A. Umpleby, N. Shah, V. Vinje, et al., 2013, Anisotropic 3D full-waveform inversion: Geophysics, **78**, no. 2, R59–R80, https://doi.org/10.1190/geo2012-0338.1.

Weickert, J., 1998, Anisotropic diffusion in image processing: B.G. Teubner.